



Effects of silicon concentration on the magnetic and structural properties of nanostructured Fe-Si alloy synthesized by ball mill process

M'hamed Ouadah^{1,2} · Abderrahmane Younes³

Received: 4 May 2023 / Accepted: 6 June 2023 / Published online: 17 June 2023
© The Author(s), under exclusive licence to Springer-Verlag London Ltd., part of Springer Nature 2023

Abstract

This study aims to elaborate on the production of a nanostructured Fe-Si alloy with varying silicon concentrations and how it can enhance the magnetic properties of the alloy. In order to achieve this, the mechanical alloying technique was employed to create the nanostructured alloy. After the mechanical ball milling process, the morphological, structural, and magnetic properties of the alloy were thoroughly analyzed using advanced techniques such as scanning electron microscopy (SEM) coupled with energy-dispersive spectroscopy (EDS), X-ray diffraction (XRD), and vibrating sample magnetometer (VSM). The results from these techniques revealed significant changes in the properties of the alloy. One of the major findings of this study was the appearance of Fe₃Si phase, commonly known as Suessite, after the mechanical milling process. This indicates that the milling process caused a transformation in the crystal structure of the alloy. Additionally, an increase in silicon concentration led to a reduction in crystallite sizes, which was observed through the XRD analysis. Furthermore, the lattice strain and lattice parameters of the alloy were observed to increase with increasing silicon concentration until it reached 3%. After this point, the value of the lattice parameter remained constant, indicating that further increases in silicon concentration did not significantly impact the lattice structure of the alloy. The FTIR analysis revealed the presence of a distinct band at 1070 cm⁻¹, indicating the occurrence of stretching vibrations associated with Fe-Si bonds. The milled samples exhibit improved magnetic properties, with increased saturation magnetization values observed as the silicon concentration increased.

Keywords Nanostructured FeSi · Fe₃Si phase · Si concentration · Structural properties · Magnetic behavior

1 Introduction

Nanostructured materials have captured the attention of researchers due to their remarkable properties, surpassing those of conventional materials [1, 2]. These materials exhibit impressive combinations of strength, toughness, and magnetic and mechanical properties [3–5]. Recently, there has been an increased interest in producing bulk

nanocrystalline parts, leading to the development of various processes [6, 7]. Of particular significance is the production of nanocrystalline materials using mechanical alloying, which has been the subject of intense research over the past decade [8, 9]. Mechanical alloying has proven to be a successful technique for producing nanostructured materials [10], offering significant potential for magnetic applications. The utilization of nanostructured FeSi is justified due to its remarkable properties, which encompass high saturation magnetization, low coercivity, and exceptional soft magnetic behavior; these distinctive characteristics make FeSi alloy an ideal choice for various applications [11–13]. These characteristics make FeSi a promising candidate for various technological applications, such as magnetic sensors, transformers, and motors. Furthermore, the nano-structuring of FeSi can further enhance these properties, making it an even more attractive material for use in advanced technological applications [14, 15].

✉ Abderrahmane Younes
younesabdo11@gmail.com

¹ National Polytechnic of Algeria: Ecole Nationale Polytechnique, 10 Rue des Frères OUDEK, 16200 El Harrach, Algeria

² Higher School of Applied Sciences of Algiers, P.O. Box 474, Place des Martyrs, 16001 Algiers, Algeria

³ Research Center in Industrial Technologies (CRTI), Cheraga, 16014 Algiers, Algeria

The aim of this study is to synthesize nanostructured Fe-Si alloys with varying silicon concentrations (ranging from 1 to 6%) and investigate their magnetic properties. The primary objective is to examine how changes in the silicon concentration affect the structural properties and magnetic behavior of the alloy when subjected to a mechanical alloying process. The study will employ advanced characterization techniques such as scanning electron microscopy (SEM), energy-dispersive spectroscopy (EDS), X-ray diffraction (XRD), and vibrating sample magnetometer (VSM) to analyze the morphological, structural, and magnetic properties of the Fe-Si samples. By exploring the relationship between the silicon concentration, crystal structure, and magnetic properties of the alloy, this research aims to develop a deeper understanding of how nanostructuring and varying silicon content can influence the performance of Fe-Si alloys. The ultimate goal is to provide valuable insights for the development of Fe-Si alloys with enhanced magnetic properties, which hold significant potential for applications in magnetic devices and related fields.

2 Materials and experimental procedures

In this study, Fe-Si nanostructured alloys were fabricated using the mechanical alloying process. The preliminary powders used in this process have a mean particle size of 60 μm for both Fe and Si. The powders were then milled in a planetary ball mill PM400 for 20 h under a controlled atmosphere using hard chromium balls. The obtained alloy compositions were $\text{Fe}_{100-x}\text{Si}_x$ (where $x = 0, 3, 4, 5,$ and 6), with a mass ratio of 1:20. Chemical bond changes were assessed using ATR spectroscopy (Agilent CARY 360 SPECTROMETER) over a wavenumber range of 400 to 4000 cm^{-1} , employing a resolution of 4 cm^{-1} and a minimum of 32 scans. To characterize the obtained milled samples, advanced techniques were utilized, including Gemini scanning electron microscopy (SEM) attached with energy-dispersive X-ray analysis unit (EDX), X-ray XPERT PRO diffractometer using $\text{Co K}\alpha$ radiation, and micro-sense vibrating sample magnetometer with a maximum applied field of 22 kOe. These techniques enabled the examination of the morphological, structural, and magnetic properties of the alloy.

3 Results and discussion

3.1 Powder structural state

The X-ray diffraction analysis of the samples subjected to mechanical milling is presented in Fig. 1, which depicts the various phases detected during the process. The characterization results reveal that the peaks corresponding to Si have

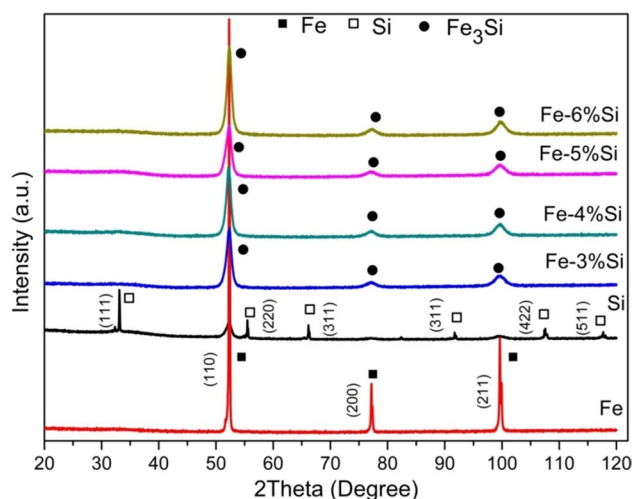


Fig. 1 X-ray diffraction analysis of the FeSi alloy as a function of varying silicon concentrations

vanished for different silicon concentrations after 20 h of milling. Interestingly, the X-ray diagram reveals the presence of only intermetallic structures Fe_3Si peaks. This finding aligns with prior studies that have similarly documented the emergence of an Fe_3Si phase throughout the mechanical alloying procedure of the FeSi alloy [16–20]. Similarly, Grognet et al. found the formation of Fe_3Si phase using the rapid quenching technique [21, 22]. The consistency of these findings underscores the importance of the Fe_3Si phase in the mechanical milling process and its potential applications in the development of new materials.

The crystallite size (D) and lattice strain (ϵ) were determined by analyzing the full width at half maximum (FWHM) using the Scherrer equation, as shown in Eqs. 1 and 2, respectively [23, 24]. These calculations are crucial in understanding the physical properties of the materials under investigation, as they provide valuable information on their microstructural characteristics. The Scherrer equation is a widely accepted method for calculating the crystallite size and lattice strain, which has been extensively used in various research studies owing to its accuracy and reliability. Therefore, by utilizing this equation, the researchers were able to obtain vital information on the microstructure of the materials, which can help in elucidating their physical and chemical properties.

$$D = \frac{K\lambda}{FWHM \tan \theta} \quad (1)$$

$$\epsilon = \frac{FWHM}{4 \tan \theta} \quad (2)$$

where D is the average crystallite size, ϵ is lattice strain, λ is the wavelength of X-ray radiation ($\lambda = 1.78901 \text{ \AA}$), K

is the Scherrer constant ($K = 0.89$), θ is the Bragg diffraction angle, and FWHM is the full width at half maximum

In the grinding process of nanostructured materials, the broadening of peaks observed in X-ray diffraction (XRD) results is attributed to two factors: the reduction in crystallite size and the increase in lattice strain [25–27].

To determine the lattice parameter (a) of the Fe_3Si phases, the researchers utilized Eq. 3 [22, 23], which is specifically designed for calculating the lattice parameter of the (110) plane. This approach is particularly useful in elucidating the crystal structure of the material and can provide critical insights into its properties. The (110) plane is an essential crystallographic orientation, and its lattice parameter is often used as a key indicator of the quality and performance of the material. By utilizing this equation, the researchers were able to obtain precise measurements of the lattice parameter, which helped them to better understand the structural characteristics of the Fe_3Si phases. Furthermore, these findings can aid in the development of novel materials with improved properties by providing valuable information on their crystal structures.

$$\frac{1}{d^2} = \frac{h^2 + k^2 + l^2}{a^2} \quad (3)$$

Figure 2 depicts the evolution of crystallite size and lattice strain for an FeSi alloy subjected to 20 h of milling at different silicon concentrations, specifically at the principal peak (110). The results indicate a rapid reduction in crystallite size from 0 to 3% Si concentration, followed by a gradual decrease from 3 to 6% Si concentration. This trend can be attributed to the enhanced crystallized volume fraction with increasing silicon content, leading to a smaller average size of the crystallites. Conversely, lattice strain experiences a rapid increase up to 3% Si concentration, followed by a slower increase beyond 3%. The initial spike can be attributed to the

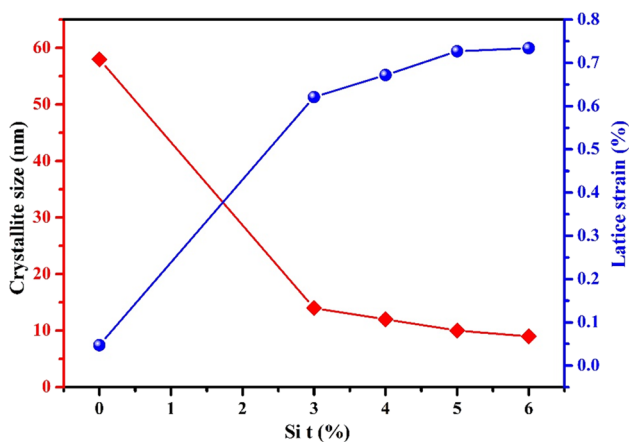


Fig. 2 Variation of crystallite size and lattice strain as a function of different silicon concentrations

formation of Fe_3Si phase, whereas the subsequent increase is due to dislocations in the crystal lattice induced by the severe plastic deformation during milling. The high density of dislocations triggers lattice distortion, thereby affecting the lattice strain [28–30]. Overall, the data in Fig. 2 suggest that the crystallite size and lattice strain of FeSi alloy are highly dependent on the silicon concentration, as well as on the extent of plastic deformation induced by milling.

Figure 3 illustrates the variation of lattice parameters as a function of different silicon concentrations. The curve can be divided into two parts: the first part ranges from 0 to 3% Si concentration, where the lattice parameters increase rapidly. This trend can be attributed to the insertion of Si atoms into the lattice of Fe, leading to a lattice expansion. In the second part, there is no significant change in the lattice parameters of Fe-Si alloy, which suggests that the lattice structure reaches a stable state beyond a certain Si concentration. The lattice parameter value obtained from the curve is 0.286 nm, which corresponds to a Si concentration in Fe-Si alloy of approximately 3–6 wt% [31, 32].

These findings provide crucial information for designing and optimizing Fe-Si alloys with specific lattice structures and properties. In summary, the results from Fig. 3 demonstrate the effect of silicon concentration on the lattice parameters of Fe-Si alloys. The observed trends can be attributed to the insertion of Si atoms into the lattice, leading to changes in the lattice expansion. These findings have implications for a wide range of applications that rely on the properties of metallic alloys [33, 34].

3.2 FTIR analysis

Figure 4 displays the FTIR spectra of Fe and Fe-Si samples. The spectral analysis of various FeSi samples exhibits

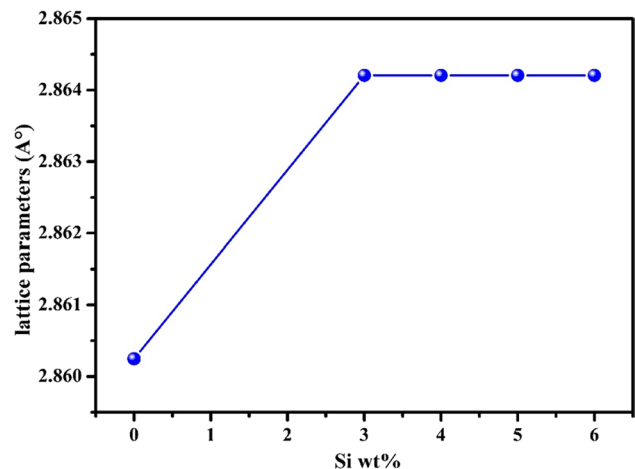


Fig. 3 Variation of lattice parameters as a function of different silicon concentrations

remarkable similarity, although minor differences can be observed in the details. These differences may be attributed to variations in the preparation conditions, Fe/Si ratios, and surface structural variances among the Fe-Si oxides. Across all the spectra, prominent absorption bands were observed at approximately ~ 3442 , ~ 3026 , ~ 2925 , ~ 2614 , ~ 2323 , ~ 2115 , ~ 1725 , ~ 1636 , ~ 1497 , ~ 1380 , ~ 1245 , and ~ 1070 cm^{-1} .

In the study conducted by Lefki et al. [35], a band at 1070 cm^{-1} was identified, corresponding to the stretching vibrations of Fe-Si. Niyonshuti et al. [36] demonstrated that the peak observed at 1497 cm^{-1} can be attributed to the shearing vibration of N-H bonds. Additionally, the signals at approximately 3442 cm^{-1} and 1636 cm^{-1} were assigned to the stretching vibration absorption of O-H bonds from water and ethanol molecules [37, 38]. Nguyen et al. [39] concluded that the carbonyl peaks of citric acid shifted to 1725 cm^{-1} upon reaction with the silicon nanoparticle surface, indicating the conversion to silyl esters (-Si-O-C(O)-C-). Poljansek et al. [40] observed several characteristic peaks in the infrared spectrum, including an unsaturated C-H stretching peak at 3026 cm^{-1} and a phase stretching vibration of CH₂-alkane at 2925 cm^{-1} . Furthermore, the presence of O-H groups was indicated by a peak at 1380 cm^{-1} , and a peak at 1245 cm^{-1} indicated the presence of Si-CH₃ groups.

3.3 Powder morphology

Figure 5 presents the morphological features of the FeSi alloy subjected to 20 h of milling at different silicon concentrations. After 20 h of milling, the particles of all samples exhibited irregular shapes and were flattened with varying sizes. This morphology can be attributed to the severe plastic deformation induced by milling.

Notably, the silicon particles were welded and fractured with iron particles to form a nanostructured FeSi alloy.

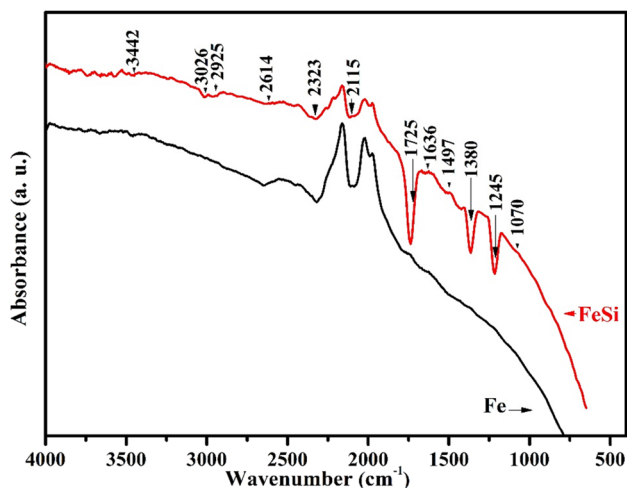


Fig. 4 FTIR spectra of Fe and FeSi milled powder alloy

The nanostructure of the Fe-Si alloy can be attributed to the reduction in grain size induced by milling. In particular, the mean grain size of the Fe-Si binary alloy is smaller than that of pure iron and pure silicon. The reduced grain size and increased grain boundary area of the nanostructured FeSi alloy could enhance its mechanical properties, such as strength and hardness. Overall, the morphological analysis presented in Fig. 4 provides further insights into the microstructural evolution of FeSi alloys under milling. These findings have important implications for the design and optimization of metallic alloys with specific morphological and microstructural features [41–44].

3.4 EDS analysis

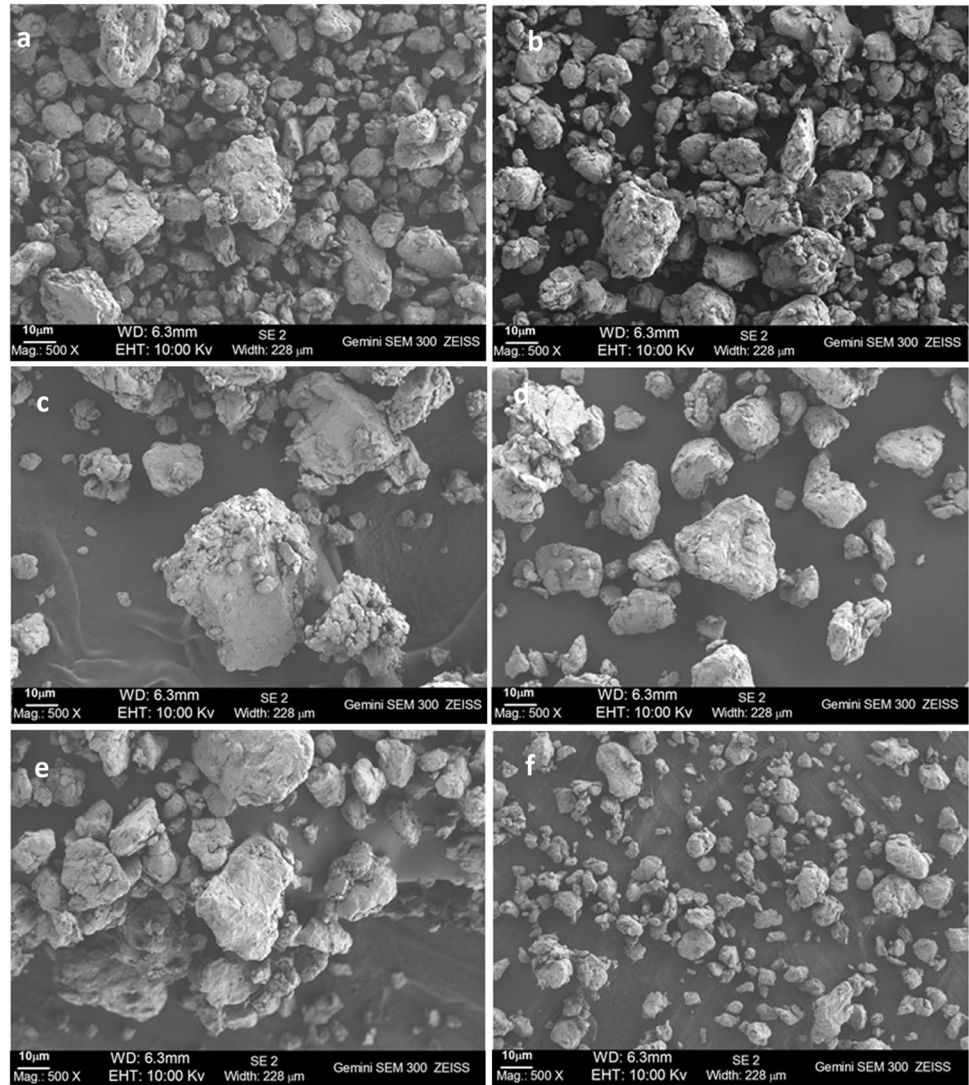
Figure 6 displays the energy-dispersive X-ray spectroscopy (EDS) spectrum of FeSi alloys with varying silicon concentrations from 0 to 5 wt%. The spectrum features different chemical elements with varying concentrations that constitute the mixture in the FeSi alloy. The EDS analysis confirms the presence of the main elements in the alloy without any significant contamination or impurity. The EDS spectrum provides valuable information about the elemental composition of the FeSi alloys. Specifically, it can identify the presence of minor elements and impurities that may affect the properties of the alloy. Additionally, the EDS spectrum can be used to quantify the relative concentrations of different elements, which is critical for alloy design and optimization. In summary, the EDS analysis presented in Fig. 6 confirms the elemental composition of the FeSi alloy and provides important information for alloy characterization and optimization [45, 46]. These findings have important implications for the development of metallic alloys with specific chemical and elemental features.

3.5 Magnetic characterization

The magnetization versus magnetic field curves, $M(H)$, for the as-milled nanostructured FeSi alloy powders are presented in Fig. 7. These curves show the characteristic hysteresis loops of a ferromagnetic material, indicating that the material is ferromagnetic. The curves were obtained by measuring the magnetization of the powders at room temperature and varying the applied magnetic field.

The graph in Fig. 8 illustrates that the saturation magnetization of the FeSi alloy decreases as the Si content increases. This phenomenon can be explained by the presence of diamagnetic Si ions in close proximity to Fe ions, which leads to a reduction in the overall magnetic moment of the material. The Si ions do not possess any unpaired electrons, which makes them diamagnetic and their presence causes a disruption in the ferromagnetic ordering of the Fe ions. As a result, the magnetic moment of the alloy is weakened,

Fig. 5 Morphology of the FeSi alloy milled at 20 h for different silicon concentration: **a** Fe, **b** Si, **c** Fe-3%Si, **d** Fe-4%Si, **e** Fe-5%Si, and **f** Fe-6%Si



leading to a decrease in the saturation magnetization. This finding is consistent with the previous literature, which has also reported a similar trend between the Si content and the saturation magnetization of FeSi alloys [47–49].

Figure 8 illustrates the variation of coercivity as a function of Si content. It is observed that the coercivity of FeSi is significantly higher than that of Fe. However, it is important to note that several factors can influence the coercivity of the material. The previously discussed lattice strain, as well as underestimation of grain size and uniformity, can all affect the coercivity. The research by Li et al. demonstrates that the grain size, grain size distribution, and grain boundary chemistry can all have a significant impact on coercivity [50, 51]. The presence of defects such as dislocations, grain boundaries, inclusions, and voids can also contribute to coercivity. In polycrystalline materials, the interaction of domain walls with grain boundaries is a major factor that influences coercivity. As the grain size decreases, the larger volume fraction

of grain boundaries leads to an increase in coercivity due to the impeding effect of boundaries on domain wall (Bloch wall) motion. It is worth noting that the magnetocrystalline anisotropy has a reduced effect on minimizing coercivity in this case [52, 53].

The magnetization remanence (Fig. 9) of FeSi is larger than Fe because of the presence of Si atoms in the alloy. As Si is introduced into the Fe lattice, it creates local magnetic moments that are opposite in direction to the Fe moments. This results in a reduction of the net magnetic moment of the Fe atoms, which decreases the overall magnetization of the alloy.

However, the presence of these Si-induced moments in FeSi also causes an increase in the magnetization remanence, as these moments tend to align with the external magnetic field and maintain their orientation even after the field is removed. The magnetization remanence of FeSi varies with changes in Si content. As the Si content increases,

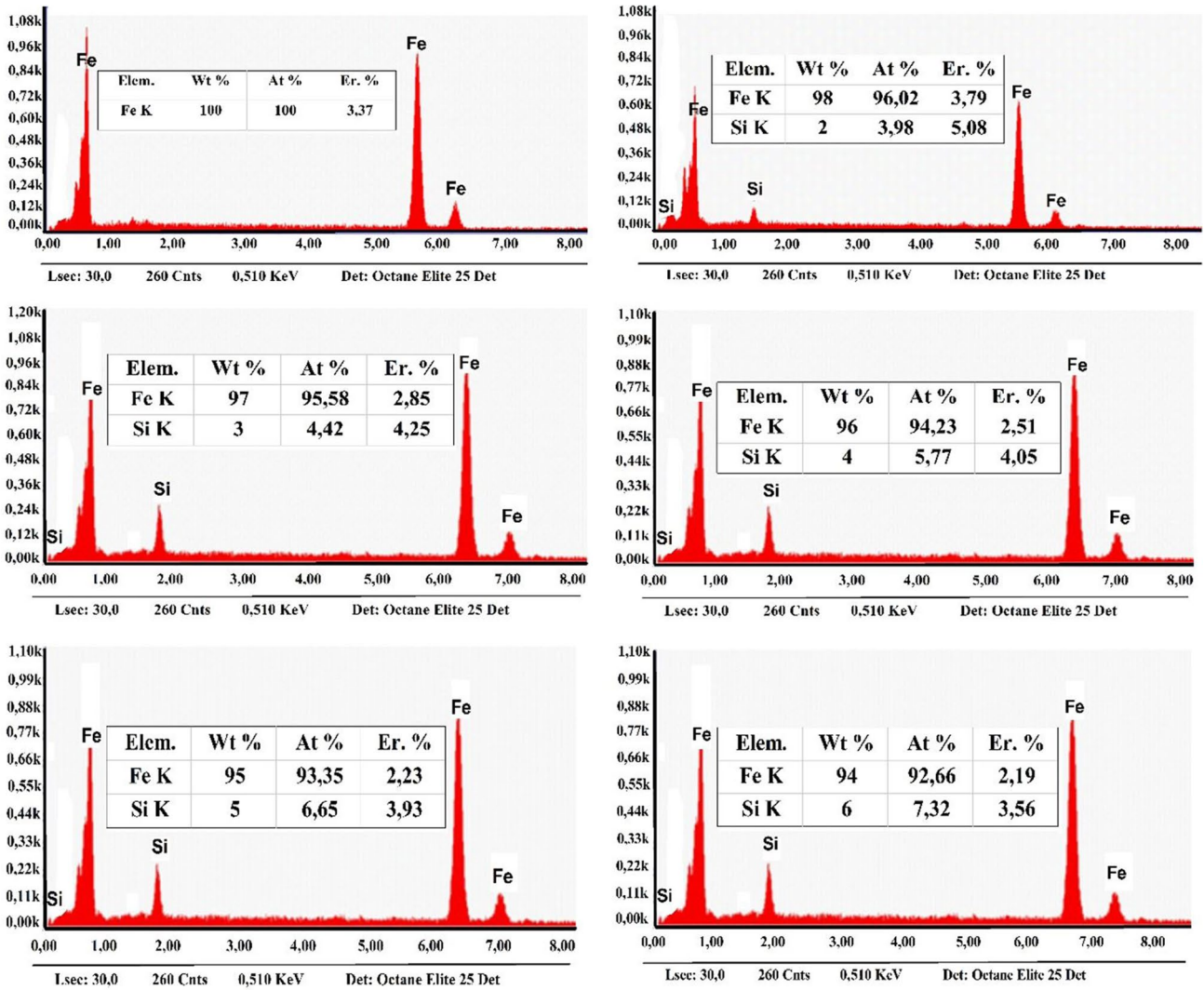


Fig. 6 EDS spectrum of nanostructured FeSi alloy with different silicon concentration

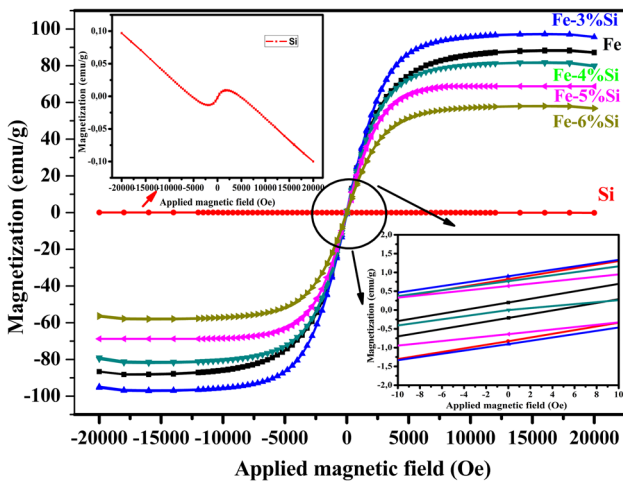


Fig. 7 Hysteresis loops of the nanostructured FeSi alloy milled at 20 h for different Si concentration

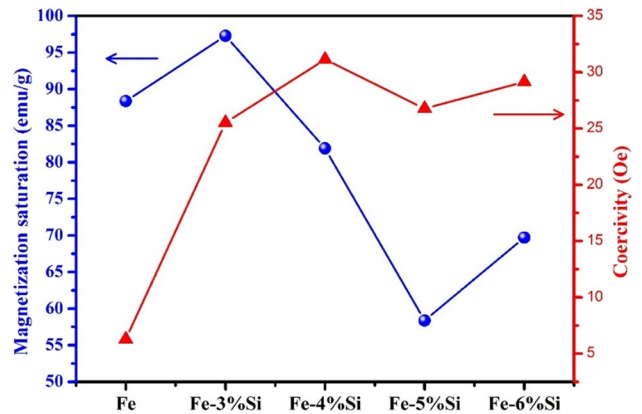


Fig. 8 Coercivity and magnetization saturation changes of the nanostructured FeSi alloy milled at 20 h for different Si concentration

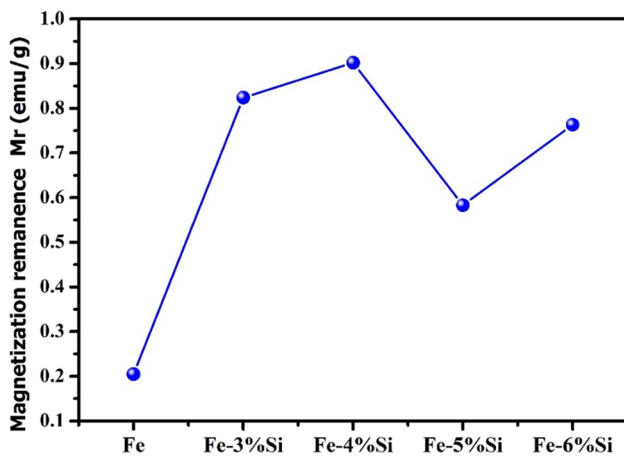


Fig. 9 Magnetization remanence changes of the nanostructured FeSi alloy milled at 20 h for different Si concentration

the magnetization remanence initially increases due to the aforementioned effect of Si-induced moments. However, at higher Si concentrations, the magnetization remanence starts to decrease, as the diamagnetic Si ions begin to disrupt the ferromagnetic ordering of the Fe ions, leading to a reduction in the overall magnetic moment of the alloy. Therefore, the variation of Si content can have a significant impact on the magnetization remanence of FeSi [54, 55].

4 Conclusion

In conclusion, this study successfully demonstrated the production of a nanostructured Fe-Si alloy with varying silicon concentrations and its consequent enhancement of magnetic properties through mechanical ball milling. Utilizing advanced techniques, the analysis of the morphological, structural, and magnetic properties of the alloy yielded significant changes, including the appearance of the Fe₃Si phase after the milling process, indicating a transformation in the crystal structure of the alloy. Furthermore, increasing the silicon concentration led to a reduction in crystallite sizes and lattice strain, with lattice parameters observed to increase until reaching 3%, beyond which further increases did not significantly impact the lattice structure. The FTIR analysis clearly demonstrated the existence of a prominent band at 1070 cm⁻¹, unequivocally indicating the presence of robust stretching vibrations attributed to the Fe-Si bonds. This finding provides valuable insights into the molecular composition and structural characteristics of the investigated material, further enriching our understanding of the Fe-Si system. The milled samples exhibited improved magnetic properties, with increasing saturation magnetization values observed with higher silicon concentration. These findings provide valuable insights into the relationship between the

structural and morphological properties of Fe-Si alloys and their magnetic behavior, thereby offering a foundation for the development of enhanced magnetic devices.

Declarations

Ethical statement The manuscript has not been submitted to more than one publication for simultaneous consideration. The submitted work is original and has not been published elsewhere in any form or language.

Conflict of interest The authors declare no competing interests.

References

- Suryanarayana C (2002) Nanostructured intermetallics. In: Intermetallic Compounds-Principles and Practice: Progress, vol 3, pp 749–764. <https://doi.org/10.1002/0470845856>
- Mazaleyrat F, Varga LK (2001) Thermo-magnetic transitions in two-phase nanostructured materials. *IEEE Trans Magn* 37(4):2232–2235. <https://doi.org/10.1109/20.951133>
- Rempel A (2007) Nanotechnologies. Properties and applications of nanostructured materials. *Russ Chem Rev* 76(5):435. <https://doi.org/10.1070/RC2007v076n05ABEH003674>
- Strečková M, Fúzer J, Kobera L, Brus J, Fáberová M, Bureš R, Bat'Ko I (2014) A comprehensive study of soft magnetic materials based on FeSi spheres and polymeric resin modified by silica nanorods. *Mater Chem Phys* 147(3):649–660. <https://doi.org/10.1016/j.matchemphys.2014.06.004>
- Gleiter H (2000) Nanostructured materials: basic concepts and microstructure. *Acta Mater* 48(1):1–29. [https://doi.org/10.1016/S1359-6454\(99\)00285-2](https://doi.org/10.1016/S1359-6454(99)00285-2)
- Enayati MH, Mohamed FA (2014) Application of mechanical alloying/milling for synthesis of nanocrystalline and amorphous materials. *Int Mater Rev* 59(7):394–416. <https://doi.org/10.1179/1743280414Y.0000000036>
- Chaudhary V, Mantri SA, Ramanujan RV, Banerjee R (2020) Additive manufacturing of magnetic materials. *Prog Mater Sci* 114:100688. <https://doi.org/10.1016/j.pmatsci.2020.100688>
- Suryanarayana C (2001) Mechanical alloying and milling. *Prog Mater Sci* 46(1-2):1–184. [https://doi.org/10.1016/S0079-6425\(99\)00010-9](https://doi.org/10.1016/S0079-6425(99)00010-9)
- Hajalilou A, Kianvash A, Lavvafi H, Shamel K (2018) Nanostructured soft magnetic materials synthesized via mechanical alloying: a review. *J Mater Sci Mater Electron* 29:1690–1717. <https://doi.org/10.1007/s10854-017-8082-0>
- Koch C (1997) Synthesis of nanostructured materials by mechanical milling: problems and opportunities. *Nanostructured Mater* 9(1-8):13–22. [https://doi.org/10.1016/S0965-9773\(97\)00014-7](https://doi.org/10.1016/S0965-9773(97)00014-7)
- Bi X, Lan W, Ou S, Gong S, Xu H (2003) Magnetic and electrical properties of FeSi/FeSi-ZrO₂ multilayers prepared by EB-PVD. *J Magn Magn Mater* 261(1-2):166–171. [https://doi.org/10.1016/S0304-8853\(02\)01469-5](https://doi.org/10.1016/S0304-8853(02)01469-5)
- Wang J, Song S, Sun H, Xue Z (2021) Improvement of magnetic properties for FeSi/FeSiAl compound soft magnetic composites by introducing impact of powder size matching. *J Mater Sci Mater Electron* 32:8545–8556. <https://doi.org/10.1007/s10854-021-05488-3>
- Balakrishna AR, James RD (2021) A tool to predict coercivity in magnetic materials. *Acta Mater* 208:116697. <https://doi.org/10.1016/j.actamat.2021.116697>

14. Dascalu M, Cesura F, Lev G, Diéguez O, Kohn A, Goldfarb I (2019) Controlling the supermagnetic response of tetragonal α -FeSi₂ nanoislands. *Appl Surf Sci* 476:189–197. <https://doi.org/10.1016/j.apsusc.2019.01.079>
15. Du VA, Sidorenko A, Bethge O, Paschen S, Bertagnolli E, Schubert U (2011) Iron silicide nanoparticles in a SiC/C matrix from organometallic polymers: characterization and magnetic properties. *J Mater Chem* 21(33):12232–12238 <https://doi.org/10.1039/C1JM11099C>
16. Zhou T, Zhang J, Xu J, Yu Z, Gu G, Wang D, Huang H, Du Y, Wang J, Jiang Y (1996) Preparation of nanocrystalline Fe-Si alloys and their magnetic properties. *J Magn Mater* 164:219. [https://doi.org/10.1016/S0304-8853\(96\)00384-8](https://doi.org/10.1016/S0304-8853(96)00384-8)
17. Parzych G, Jankowska-Kisielinska J, Dobrzyński L (2010) Magnetic properties of DO₃-type alloys based on Fe₃Si and Fe₃Al. *Acta Physica Polonica A* 117(4):578–581. <https://doi.org/10.12693/APhysPolA.117.578H>
18. Atmani H, Grognet S, Teillet J (2001) Crystallization-nitriding process of FeSiB and FeSiBCuNb ribbons: influence of additive (Cu,Nb) pair and nitrogen on structure, magnetic and magnetostrictive parameters. *J Non Cryst Solids* 290(2-3):194–207. [https://doi.org/10.1016/S0022-3093\(01\)00737-2](https://doi.org/10.1016/S0022-3093(01)00737-2)
19. Akinwamide SO, Lemika SM, Abiodun B (2019) Study of microstructural and mechanical properties of stir cast Al (SiC-Mg-TiFe) composite. *Fluid Dyn Mater Process* 15(1):15–26. <https://doi.org/10.32604/fdmp.2019.04761>
20. Akinwamide SO, Akinribide OJ, Olubambi PA (2021) Microstructural evolution, mechanical and nanoindentation studies of stir cast binary and ternary aluminium based composites. *J Alloys Compd* 850:156586. <https://doi.org/10.1016/j.jallcom.2020.156586>
21. Gao ZQ, Fultz B (1994) Thermal stability of Fe₃Si-based nanocrystals. *Hyperfine Interact* 94:2213–2218. <https://doi.org/10.1007/BF02063764>
22. Grognet S, Le Breton JM, Atmani H, Teillet J (2000) Microstructural study of nanocrystalline Fe-(Cu-Nb)-Si-B ribbons obtained by a nitriding thermochemical treatment. *J Magn Mater* 210:167–180. [https://doi.org/10.1016/S0304-8853\(99\)00763-5](https://doi.org/10.1016/S0304-8853(99)00763-5)
23. Dilmi N, Bacha NE, Younes A (2020) Structural and magnetic properties of Fe_{60-x}Ni_x(ZnO) 40 nanocomposites produced by mechanical milling and coated by thermal spraying on a steel substrate. *Powder Metallurgy and Metal Ceramics* 59:35–45. <https://doi.org/10.1007/s11106-020-00136-7>
24. Younes A, Khorchef M, Bouamer A, Amar H (2019) Magnetic and structural behavior of Fe-CoO nanocomposites mechanically milled. *IOP Conf Ser: Mater Sci Eng* 557:012064. <https://doi.org/10.1088/1757-899X/557/1/012064>
25. Soni PR (2000) *Mechanical alloying: fundamentals and applications*. Cambridge Int Science Publishing
26. Suryanarayana C (2008) Recent developments in mechanical alloying. *Rev Adv Mater Sci* 18(3):203–211
27. Herr U (1995) Mechanical alloying and milling. In: *Key engineering materials*, vol 103. Trans Tech Publications Ltd., pp 113–124
28. Sanin VN, Ikornikov DM, Andreev DE, Sachkova NV, Yukhvid VI (2019) Mill scale recycling by SHS metallurgy for production of cast ferrosilicon and ferro-silico-aluminium. *IOP Conf Ser: Mater Sci Eng* 558:012041. <https://doi.org/10.1088/1757-899X/558/1/012041>
29. Piamba JF, Rodríguez R, Alcázar GP (2012) Mössbauer and XRD study of the Fe_{0.5}Si_{0.5} system produced by mechanical alloying and sinterization. *Revista Mexicana de Física* 58(2):88–92 <https://www.redalyc.org/articulo.oa?id=57030392023>
30. Abbassi L, Mesguich D, Berthebaud D, Le Tonquesse S, Srinivasan B, Mori T, Beaudhuin M (2021) Effect of nanostructuring on the thermoelectric properties of β -FeSi₂. *Nanomaterials* 11(11):2852. <https://doi.org/10.3390/nano11112852>
31. Yamada H, Katsumata H, Yuasa D, Uekusa S, Ishiyama M, Souma H, Azumaya I (2012) Structural and electrical properties of β -FeSi₂ bulk materials for thermoelectric applications. *Phys Procedia* 23:13–16. <https://doi.org/10.1016/j.phpro.2012.01.004>
32. Piamba JF, Ortega C, Hernández-Bravo R, Carmona JG, Tabares JA, Alcázar GP, Alvarado-Orozco JM (2020) Theoretical and experimental study of FeSi on magnetic and phase properties. *Appl Phys A* 126:1–9. <https://doi.org/10.1007/s00339-020-04038-8>
33. Cherigui M, Guessasma S, Fenineche N, Hamzaoui R, El-Kedim O, Coddet C (2005) Studies of magnetic properties of iron-based coatings produced by a high-velocity oxy-fuel process. *Mater Chem Phys* 92(2-3):419–423. <https://doi.org/10.1016/j.matchemphys.2005.01.047>
34. Ma Y, Liu L, Ren X, Liu A (2018) The effect of target-substrate distance on surface morphology and properties of β -FeSi₂ films prepared by pulsed laser deposition. *IOP Conf Ser: Mater Sci Eng* 452:022153. <https://doi.org/10.1088/1757-899X/452/2/022153>
35. Lefki K, Muret P, Bustarret E, Boutarek N, Madar R, Chevrier J et al (1991) Infrared and Raman characterization of beta iron silicide. *Solid State Commun* 80(10):791–795
36. Niyonshuti II, Krishnamurthi VR, Okyere D, Song L, Benamara M, Tong X, Wang Y, Chen J (2020) Polydopamine surface coating synergizes the antimicrobial activity of silver nanoparticles. *ACS Appl Mater Interfaces* 12:40067–40077
37. Wang J, Guo Z, Zeng Q, Hang G, Xue Z, Chen D et al (2020) Magnetic properties regulation and loss contribution analysis for Fe-based amorphous powder cores doped with micron-sized FeSi powders. *Journal of Magnetism and Magnetic Materials* 510:166931
38. Sun K, Feng S, Jiang Q, Li XF, Li Y, Fan RH, An Y, Wang JQ (2020) Intergranular insulating reduced iron powder-carbonyl iron powder/SiO₂-Al₂O₃ soft magnetic composites with high saturation magnetic flux density and low core loss. *J MagnMagn Mater* 493:165705
39. Nguyen CC, Yoon T, Seo DM, Guduru P, Lucht BL (2016) Systematic investigation of binders for silicon anodes: interactions of binder with silicon particles and electrolytes and effects of binders on solid electrolyte interphase formation. *ACS Appl Mater Interfaces* 8(19):12211–12220
40. Poljansek I, Krajnc M (2005) Characterization of phenol-formaldehyde prepolymer resins by in line FT-IR spectroscopy. *Acta Chimica Slovenica* 52(3):238
41. Zhang Y, Ivey DG (1998) Fe₃Si formation in Fe-Si diffusion couples. *J Mater Sci* 33:3131–3135. <https://doi.org/10.1023/A:1004347907052>
42. Li H, Xue CL, Yang Y, Liang JL (2023) Preparation of Fe₃Si and FeSi intermetallic compounds from copper slag by electrochemical method. *J Iron Steel Res Int* 30(2):305–316. <https://doi.org/10.1007/s42243-022-00880-7>
43. Yakin A, Simsek T, Avar B, Simsek T, Chattopadhyay AK (2023) A review of soft magnetic properties of mechanically alloyed amorphous and nanocrystalline powders. *Emergent Materials*:1–29. <https://doi.org/10.1007/s42247-023-00485-0>
44. Yang YM, Loka C, Kim DP, Joo SY, Moon SW, Choi YS, Lee KS (2017) Si-FeSi₂/C nanocomposite anode materials produced by two-stage high-energy mechanical milling. *Met Mater Int* 23:610–617. <https://doi.org/10.1007/s12540-017-6510-6>
45. Vorauer T, Kumar P, Berhaut CL, Chamasemani FF, Jouneau PH, Aradilla D, Brunner R (2020) Multi-scale quantification and modeling of aged nanostructured silicon-based composite anodes. *Commun Chem* 3(1):141–152. <https://doi.org/10.1038/s42004-020-00386-x>
46. Yeh CL, Chen KT (2021) Synthesis of FeSi-Al₂O₃ composites by autowake combustion with metallothermic reduction. *Metals* 11:258. <https://doi.org/10.3390/met11020258>
47. Stanciu CD, Marinca TF, Chiciuş I, Isnard O (2017) Characterization of the Fe-10 wt% Si nanocrystalline powder obtained by

- mechanical alloying and annealing. *J Magn Magn Mater* 441:455–464. <https://doi.org/10.1016/j.jmmm.2017.06.010>
48. Overman NR, Jiang X, Kukkadapu RK, Clark T, Roosendaal TJ, Coffey G, Mathaudhu SN (2018) Physical and electrical properties of melt-spun Fe-Si (3–8 wt.%) soft magnetic ribbons. *Mater Charact* 136:212–220. <https://doi.org/10.1016/j.matchar.2017.12.019>
49. Clark T, Mathaudhu SN (2019) Microstructure and magnetic properties of dilute nanocrystalline Fe-Si prepared by high energy ball milling. *J Magn Magn Mater* 484:350–355. <https://doi.org/10.1016/j.jmmm.2019.03.070>
50. Li M, Birringer R, Johnson WL, Shull RD (1993) Nanocrystalline Fe-Si phase by mechanical attrition and its soft magnetic properties. *Nanostruct Mater* 3:407–412. [https://doi.org/10.1016/0965-9773\(93\)90106-L](https://doi.org/10.1016/0965-9773(93)90106-L)
51. Vinzelberg H, Schumann J, Elefant D, Arushanov E, Schmidt OG (2008) Transport and magnetic properties of Fe₃Si epitaxial films. *J Appl Phys* 104(9):093707. <https://doi.org/10.1063/1.3008010>
52. McHenry ME, Laughlin DE (2000) Nano-scale materials development for future magnetic applications. *Acta Mater* 48(1):223–238. [https://doi.org/10.1016/S1359-6454\(99\)00296-7](https://doi.org/10.1016/S1359-6454(99)00296-7)
53. Cunha MA, Johnson GW (1990) Rapidly solidified Si-Fe alloys. *J Mater Sci* 25(5):2481–2486. <https://doi.org/10.1007/BF00638046>
54. Salaheldeen M, Garcia-Gomez A, Corte-León P, Gonzalez A, Ipatov M, Zhukova V, Zhukov A (2022) Manipulation of magnetic and structure properties of Ni₂FeSi glass-coated microwires by annealing. <https://doi.org/10.2139/ssrn.4174945>
55. Hocine M, Guittoum A, Hemmous M, Martínez-Blanco D, Gorria P, Rahal B, Laggoun A (2017) The role of silicon on the microstructure and magnetic behaviour of nanostructured (Fe_{0.7}Co_{0.3})_{100-x}Si_x powders. *J Magn Magn Mater* 422:149–156. <https://doi.org/10.1016/j.jmmm.2016.08.058>

Publisher's note Springer Nature remains neutral with regard to jurisdictional claims in published maps and institutional affiliations.

Springer Nature or its licensor (e.g. a society or other partner) holds exclusive rights to this article under a publishing agreement with the author(s) or other rightsholder(s); author self-archiving of the accepted manuscript version of this article is solely governed by the terms of such publishing agreement and applicable law.